Science Advances
AAAS

Supplementary Materials for

Soft robotic origami crawler

Qiji Ze, Shuai Wu, Jun Nishikawa, Jize Dai, Yue Sun, Sophie Leanza, Cole Zemelka, Larissa S. Novelino, Glaucio H. Paulino*, Ruike Renee Zhao*

*Corresponding author. Email: gp1863@princeton.edu (G.H.P.); rrzhao@stanford.edu (R.R.Z.)

Published 30 March 2022, *Sci. Adv.* **8**, eabm7834 (2022)
DOI: 10.1126/sciadv.abm7834

The PDF file includes:

Other Supplementary Material for this manuscript includes the following:

Supplementary Text

1. Sample fabrication

Kresling origami. Two kinds of Kresling units with the same geometry and reverse creases are used to fabricate the two-unit Kresling dipole and four-unit crawler in this work. As shown in Fig. S1, both units have the same dimensions with a = 5.33 mm, b = 3.9 mm, c = 5.1 mm, and α = 106.89°. The units are fabricated from polyethylene film (0.05 mm thick), which is cut into a flower-shaped pattern using a mechanical cutter (Cricut Maker, Cricut, Inc., USA). The pattern is then folded, and Mylar hexagons (0.127 mm thick) are attached to the top and bottom sides of the unit to provide high stiffness.

Magnetic plate. Hard-magnetic microparticles (NdFeB, average size 100 μm, Magnequench, Singapore) are mixed homogeneously into Ecoflex-0030 precursor (Smooth-On, Inc., USA) with a volume fraction of 40%. To fabricate magnetic plates, the mixture is poured into hexagon-shaped acrylic molds (edge length of 3.9 mm and thickness of 1.4 mm) and cured at 80 °C for 0.5 h. The magnetic plates are magnetized by a home-made magnetizer with a 1.5 T impulse magnetic field before being attached to the Kresling units using Sil-poxy adhesive (Smooth-On, Inc., USA).

2. Material characterization

Magnetic material. The magnetic properties of the magnetic plates are measured using a vibrating sample magnetometer (7400A, Lake Shore Cryotronics, Inc., USA). The magnetic moments along the magnetization direction are measured using 4 mm by 4 mm by 1 mm samples. The corresponding remanent magnetization (M_r) is calculated from the magnetic moment by dividing the sample volume. The M_r of the sample with 40 vol% of magnetic particles is measured to be 227.50 kA m^{-1}.

Polyethylene film. The polyethylene film is characterized by uniaxial tensile tests using a universal testing machine (3344, Instron, Inc., USA). A 100 N load cell is used. Thin-film samples (gauge zone 15 mm by 5 mm by 0.05 mm) are stretched to 5% strain at a strain rate of 0.01 s^{-1}, as shown in Fig. S2. Its Young's modulus is calculated to be 207.9 MPa by the secant modulus at 0.5% strain.

3. Mechanical characterization of the Kresling unit

To characterize the mechanical behavior of fabricated Kresling units, we perform axial compression tests using a universal testing machine, as shown in Fig. S3A. From the cyclic compression test results of the Kresling unit in Fig. S3B, we observe that the mechanical response stabilizes after 400 cycles approximately. To obtain consistent results, all fabricated Kresling units are manually compressed 400 times prior to performing other mechanical tests and magnetic actuation. Then, three samples are compressed with 50% strain at a strain rate of 0.01 s^{-1}. Fig. S4A shows the measured force-contraction ($\Delta H/H$) curve of fabricated units, where H is the initial unit height and ΔH is the height change during compression. Stored energy is obtained by integrating the experimentally measured force-displacement results (Fig. S4B). The Kresling unit shows coupled contraction and rotation behaviors, which means that it can be folded under either a compressive force or a pair of torques. To derive the torque-rotation angle relationship from the force-contraction curve, the geometrical contraction-rotation angle (ψ) relation is needed, which is obtained by simulating the Kresling unit contraction using FEA and is shown in Fig. S4C. By

deriving the stored energy with respect to ψ, we can obtain the torque needed to fold the Kresling unit (Fig. S4D).

4. Free body diagram of the Kresling crawler

The introduced Kresling dipole with mirror symmetry demonstrates contraction while free of relative rotation between the two ends. Here we design a crawler composed of two Kresling dipoles with central symmetry arrangement as shown in Fig. S5. T_1, T_2, T_3, and T_4 are magnitudes of applied torques at the 1st, 2nd, 4th, and 5th hexagonal planes of the crawler from left to right. To realize simultaneous contraction of all units, it is required that the torque distribution fulfill three conditions.

1) Balance of torque for the pure translational motion:

$$T_1 + T_3 = T_2 + T_4, \tag{S1}$$

2) Same torque magnitude on all units for simultaneous contraction:

$$T_{U1} = T_{U2} = T_{U3} = T_{U4}, \tag{S2}$$

where T_{U1}, T_{U2}, T_{U3}, and T_{U4} are the torque magnitudes on units U1, U2, U3, and U4, respectively.

3) Sufficient torque magnitude on each unit for effective contraction. We define this torque as T_e with the value of 0.18 N·mm, which is a reasonably small torque permitting 35% contraction of units used in this work (Fig. S4D).

Based on the free body diagrams in Fig. S5, we have:

$$T_{U1} = T_1,\ T_{U2} = T_2 - T_1. \tag{S3}$$

Due to the symmetry of the structure and loadings, we have:

$$T_{U3} = T_3 - T_4,\ T_{U4} = T_4. \tag{S4}$$

Combining Eqs. S1-4, we have:

$$T_2 = 2T_1,\ T_3 = T_2,\ T_4 = T_1. \tag{S5}$$

Notice that T_1 and T_4 are in reverse directions, and similarly, T_2 and T_3 are in reverse directions.

5. Finite element analysis

The commercial software ABAQUS 2020 (Dassault Systèmes, France) is utilized for the Kresling crawler contraction finite element analysis (FEA). The model of each Kresling unit consists of three sections: hexagonal bases, triangular panels, and hinges connecting the panels and bases (Fig. S6A). Linear-elastic material models are used for all three sections. Normalized Young's moduli of 10, 40, and 1 (consistent units) are used for the bases, panels, and hinges, respectively, with the same Poisson's ratio of 0.4. The mesh of the crawler model is shown in Fig. S6B. Five elements are assigned through the thickness direction of bases, hinges, and panels. The pre-defined element C3D8 is used for the whole model.

To numerically verify the derived torque relations in Eq. S5, the boundary conditions applied to the crawler in FEA follow two requirements: 1) No rotation at two ends of the Kresling crawler

(1^{st} and 5^{th} hexagonal planes from left to right). 2) Reverse rotations with the same rotation angles at the 2^{nd} and 4^{th} hexagonal planes of the crawler from left to right. Here, we define the local *xyz* coordinate on the crawler with the *x*-axis along the axial direction of the crawler (Fig. S6B). The 3^{rd} hexagonal plane of the crawler is constrained along the *x*-axis, and central nodes of all hexagonal planes are constrained in the *y*-axis and *z*-axis. Rotation angles of 0°, 32°, -32°, and 0° around the *x*-axis are then enforced to the 1^{st}, 2^{nd}, 4^{th}, and 5^{th} hexagonal planes of the crawler from left to right (positive rotation direction follows the right-handed rule).

Reaction torques T_1, T_2, T_3, and T_4 at the 1^{st}, 2^{nd}, 4^{th}, and 5^{th} hexagonal planes of the crawler from left to right are exported, and normalized torque-rotation angle curves are shown in Fig. S6C. The torque relation from FEA (Fig. S6D) verifies the theoretically derived torque distribution in Eq. S5 for simultaneous contraction of four units.

6. Magnetic actuation setup

The crawler is actuated under a three-dimensional (3D) magnetic field, which is generated by customized 3D Helmholtz coils shown in Fig. S7. Three pairs of standard Helmholtz coils are configured orthogonally to each other. The magnetic field direction and magnitude can be manipulated by controlling the currents in three pairs of coils. The coils can generate 2.96 mT A^{-1}, 2.97 mT A^{-1}, and 2.90 mT A^{-1} uniform magnetic fields within a space of 160 mm by 120 mm by 80 mm (*X*-axis, *Y*-axis, and *Z*-axis), respectively.

7. Experimental details of the Kresling crawler

Contraction test. The magnetic field along the local *y*-axis is applied to the Kresling crawler, and its magnitude ranges from 0 to 40 mT with a 5 mT interval. In Fig. 2E, contractions are calculated as $1-\ell / L$, where L and ℓ are the lengths of the crawler at the initial state and after contraction, respectively. We test three samples, and each sample is tested three times to obtain average values and the range of responses.

Feet design. The locomotion of the crawler relies on anisotropic friction of the feet during the contraction phase and expansion phase in Fig. 3A. The feet are molded by PDMS (Sylgard 184, Dow Corning, USA, base to curing agent in a ratio of 5:1) with dimensions shown in Fig. S8A. Acetate tape is attached to the inclined surface. By design, the PDMS portion provides high friction, and the tape portion provides low friction.

Friction coefficient measurement. Locomotion of the crawler is conducted on two substrates, paper and PDMS (base to curing agent in a ratio of 5:1) with lubricant oil. We measure friction coefficients of PDMS (high friction) and tape (low friction) for the feet of the crawler on both substrates using the setup shown in Fig. S8B. The pulley and wire transmit the pulling force from the universal testing machine to a cubic sample (dimension: 15 mm × 15 mm × 10 mm). Cubes with and without tape attached to the bottom surface are tested. For each cube, three tests are conducted at a pulling speed of 40mm min^{-1}, 80 mm min^{-1}, and 160 mm min^{-1}. The friction coefficient can be calculated by dividing the average measured force by the weight of the cube sample. Fig. S8C shows that the measured friction coefficient of PDMS is higher than that of tape on both substrates, indicating the effective design of the high friction and low friction portions for the feet of the crawler.

Characterization of crawling motion. A triangular wave in Fig. S9A is first used to demonstrate the robotic crawling mechanism, as shown in Fig. 3A. To characterize the influence of the magnetic field profile on the crawling performance, triangular wave profiles (Fig. S9B) with different frequencies (1.67 Hz, 2.5 Hz, and 5 Hz) and magnitudes (10 mT to 40 mT with a step of 5 mT) are applied. The measured stride distance and crawling speed are shown in Fig. 3B and 3C, respectively. Multiple tests are conducted to obtain average values and range of responses.

"Z" crawling path. The Z-shaped path (Fig. 4B) consists of three straight segments. Segments 1 and 3 are along the *X*-axis. Segment 2 has an angle of -130° with respect to the *X*-axis. The frequency of the magnetic field profile for the crawler is 1.67 Hz. The magnetic field applied for actuation is always along the local *y*-axis of the crawler.

"O" crawling path. The crawling along the O-shaped path (Fig. 4C) is achieved by continuously changing the relative angle between the global and local coordinate systems from 0° to 360° over time. It takes 118 cycles to complete the path. The frequency of the magnetic field profile for the crawler is 1.67 Hz. The magnetic field applied for actuation is always along the local *y*-axis of the crawler.

Anisotropic structure stiffness measurement. Compression tests along both axial and lateral directions of the crawler body are carried out using a universal testing machine, as shown in Fig. S10. For the axial compression, a modified setup is used, as shown in Fig. S10A. The pulley and wire transmit the force from the universal testing machine to a slider in the electromagnetic coils to axially compress the Kresling crawler under a magnetic field (see detail in Fig. S10B). The force-displacement curves are exported with a total compressive displacement of 13 mm at a strain rate of 0.01 s^{-1}. To obtain the effective structure stiffness, we divide the displacement by the initial length of the sample (~ 28 mm) to obtain axial compressive strain and divide the force by the hexagon area (39.5 mm^2) to obtain the axial compressive stress as shown in Fig. 5B. A compression mode of the universal testing machine is used for the lateral compression without magnetic field, as shown in Fig. S10C. In this case, a total displacement of 1 mm is applied at a strain rate of 0.01 s^{-1}. We divide the displacement by the initial height of the sample (6.8 mm) to get lateral compressive strain and divide the force by the contacted area (109.2 mm^2) to get the lateral compressive stress as shown in Fig. 5C. To study the effect of the magnetic field on the lateral stiffness of the crawler, we perform the lateral compression tests under magnetic field in a modified setup based on the universal testing machine, as shown in Fig. S11A. The compression mode of the universal testing machine is used, and a total displacement of 1 mm is applied at a strain rate of 0.01 s^{-1}. The lateral compressive strain is also calculated by dividing the displacement by the initial height of the sample (6.8 mm). To calculate the lateral compressive stress, it should be noted that the contacted area changes with the applied magnetic field. When we apply the negative magnetic fields, the crawler expands, and its configuration is almost unchanged. In contrast, when we apply the positive magnetic fields, the crawler contracts, and the contact area under compression changes. The measured stress-strain curves and calculated lateral stiffnesses at 10% strain under negative and positive magnetic fields are shown in Fig. S11B and C, respectively.

Crawling motion in confined spaces. To demonstrate the crawling motion in confined spaces, the Kresling crawler is sandwiched between a soft substrate and a soft film with lubricant oil added in between. The substrate is molded by PDMS (base to curing agent in a ratio of 5:1), and the top film (0.15 mm thickness) is spin-coated by the same material at 200 rpm for 30 s. The magnetic field profile shown in Fig. 5D is applied to actuate the crawler. Due to the large lateral structure stiffness of the crawler, it can effectively overcome the lateral resistance from the confined

environment by cracking open the contacted areas and moving forward. It should be noted that a reverse magnetic field is applied at the end of each crawling cycle to further stretch the crawler and provide an enhanced stiffness along the axial direction. This high axial stiffness helps the crawler overcome the resistance from the axial direction during movement in confined spaces. The crawler exhibits axial stiffnesses of 8.2 kPa and 12.5 kPa, when no magnetic field and a negative 20 mT magnetic field are applied, respectively.

Drug storage and release. The mechanism of drug storage of the crawler is shown in Fig. 6A. All units and magnetic plates have holes with a diameter of 2.5 mm. The concentrated gel-based teal dye (Wilton Brands LLC, USA) is sealed inside the water-soluble container (SmartSolve Industries, USA) to make a pill with a length of 7.6 mm and a diameter of 2 mm. The pill is then inserted into the internal cavity of the rightmost Kresling unit. The right end of the pill is fixed to the magnetic plate using Sil-poxy adhesive.

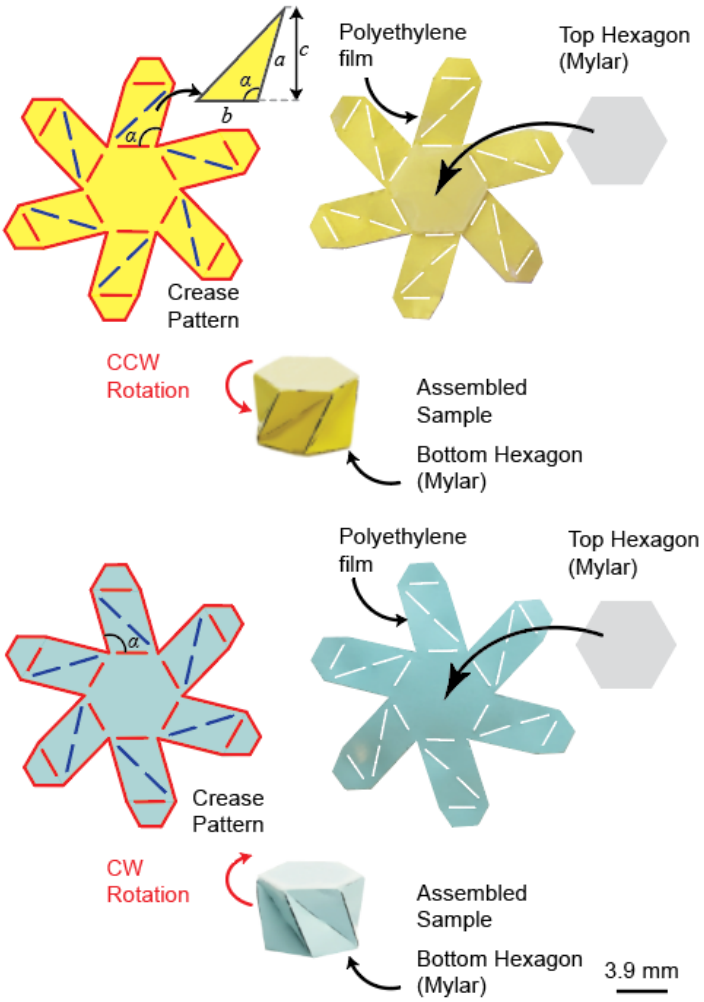

Fig. S1. Geometry, materials, and fabrication processes of Kresling units. Abbreviations CCW and CW represent counterclockwise and clockwise, respectively.

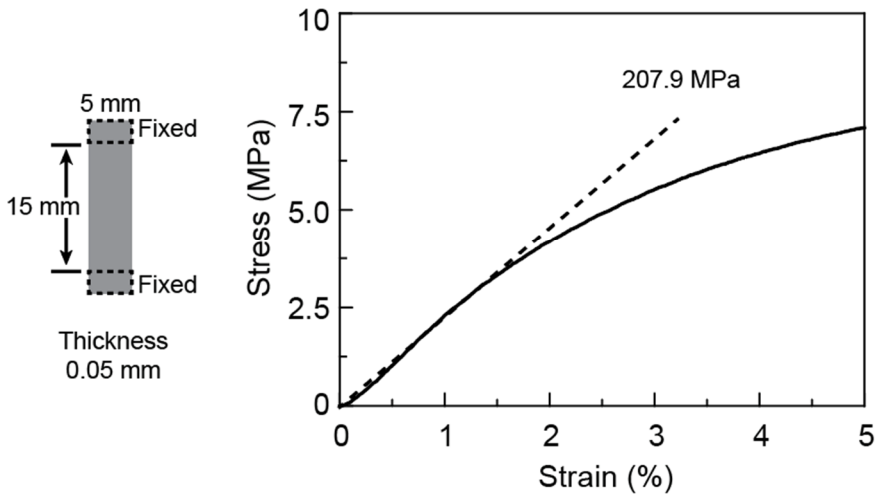

Fig. S2. Uniaxial tensile test of the polyethylene film. The polyethylene film is stretched to 5% strain at a strain rate of 0.01 s^{-1}. Its Young's modulus is calculated to be 207.9 MPa using the secant modulus at 0.5% strain.

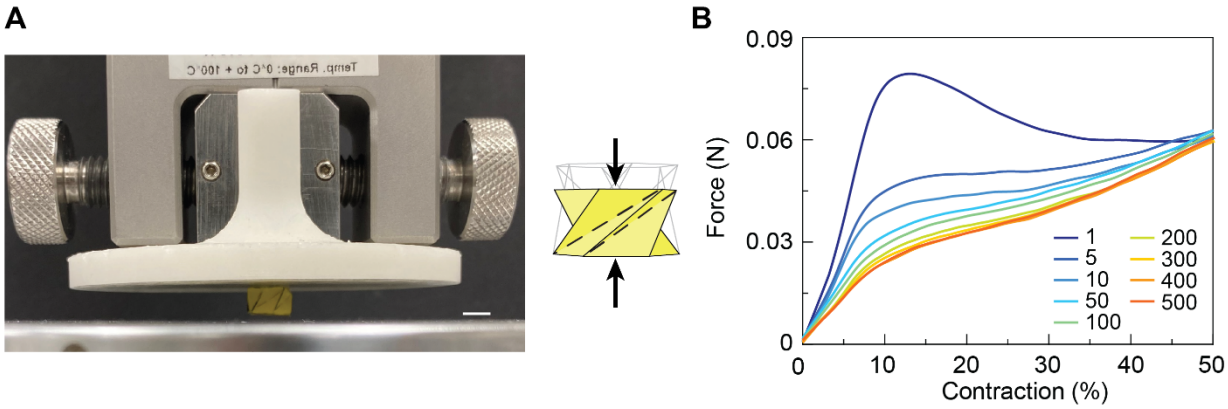

Fig. S3. Experimental setup and the measured mechanical behavior of Kresling unit under cyclic axial compression. (**A**) Compression test setup of the Kresling unit. Scale bar: 5 mm. (**B**) Force-contraction curves of Kresling unit up to 500 compression cycles. Notice that the mechanical response stabilizes after 400 cycles approximately.

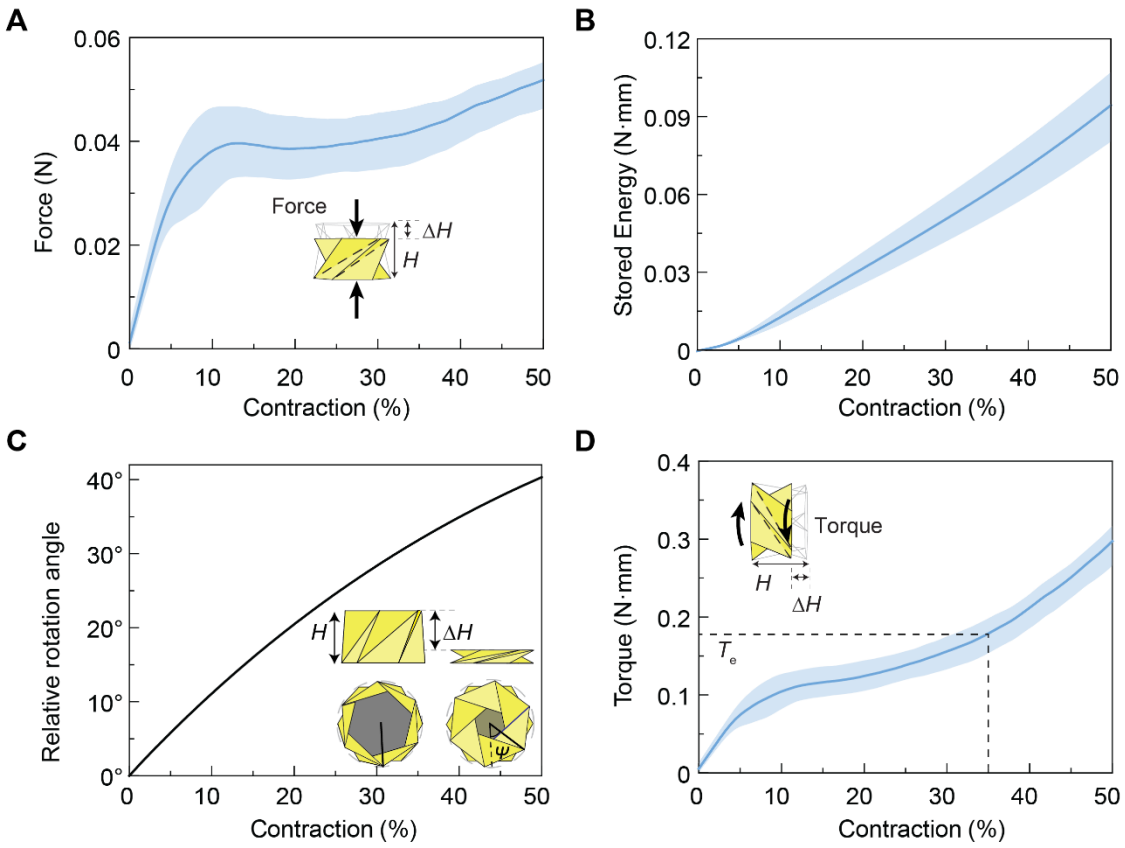

Fig. S4. Mechanical characterization of Kresling units under axial compression. (**A**) Experimental force-contraction ($\Delta H/H$) curve of fabricated Kresling units. The results are measured after manually compressing the Kresling units for 400 cycles for a stable mechanical behavior. (**B**) Stored energy-contraction curve by integrating measured force-displacement results. (**C**) Relationship between relative rotation angle ψ and contraction obtained via FEA. (**D**) Calculated torque-contraction curve. Parameter T_e is defined as the corresponding torque at 35% contraction of the unit for effective crawling motion. Solid lines are the averaged responses of three Kresling unit samples, and shaded regions represent the range of responses.

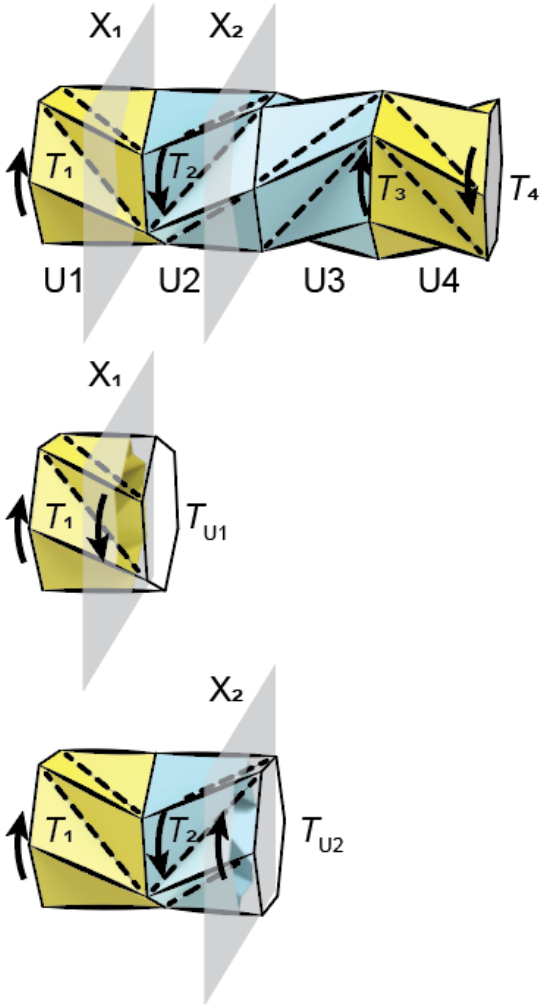

Fig. S5. Free body diagrams and torque distribution of the Kresling crawler. T_1, T_2, T_3, and T_4 are magnitudes of applied torques at the 1st, 2nd, 4th, and 5th hexagonal planes of the crawler from left to right. X_1 and X_2 are two cut-off planes on units U1 and U2, respectively. T_{U1}, T_{U2}, T_{U3}, and T_{U4} are the torque magnitudes on units U1, U2, U3, and U4, respectively.

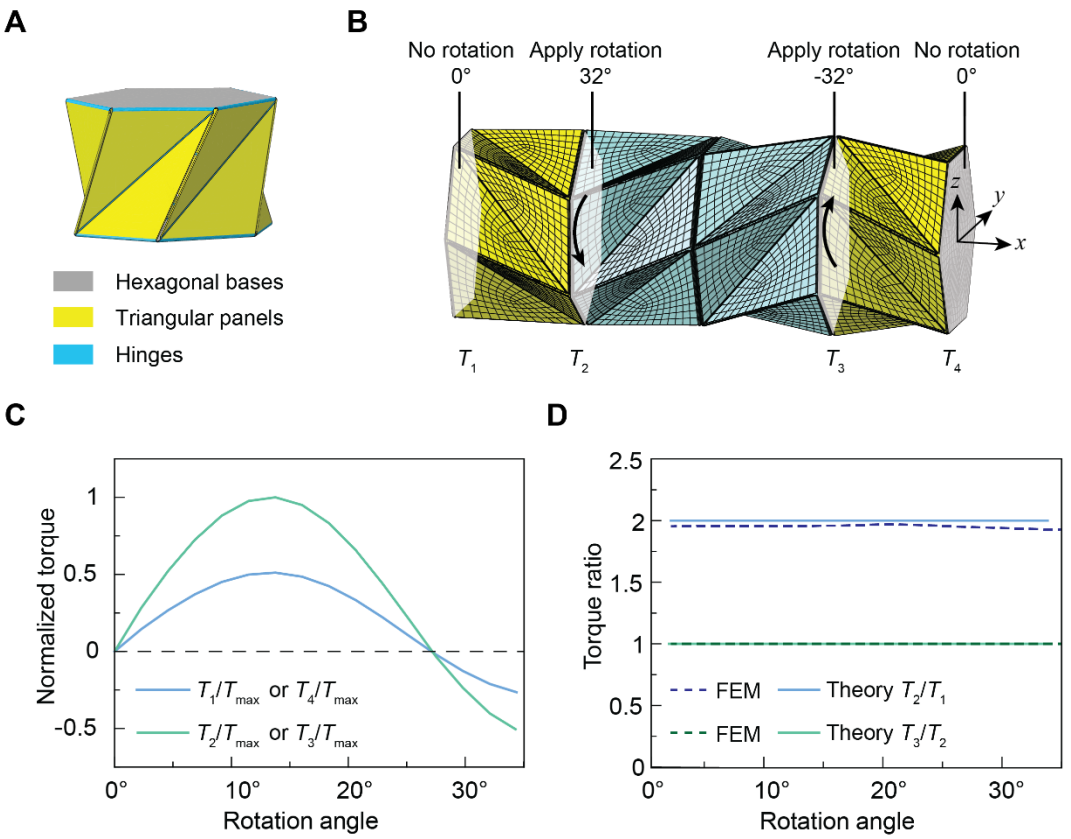

Fig. S6. Verification of torque distribution via finite element analysis (FEA). (**A**) FEA model of Kresling unit consists of three sections: hexagonal bases, triangular panels, and hinges connecting the panels and bases. (**B**) Mesh and boundary conditions of the Kresling crawler. Parameters T_1, T_2, T_3, and T_4 are magnitudes of corresponding reaction torques. (**C**) Exported normalized torque-rotation angle curves. (**D**) Comparison of torque distribution for simultaneous contraction of four units from theory and finite element simulation.

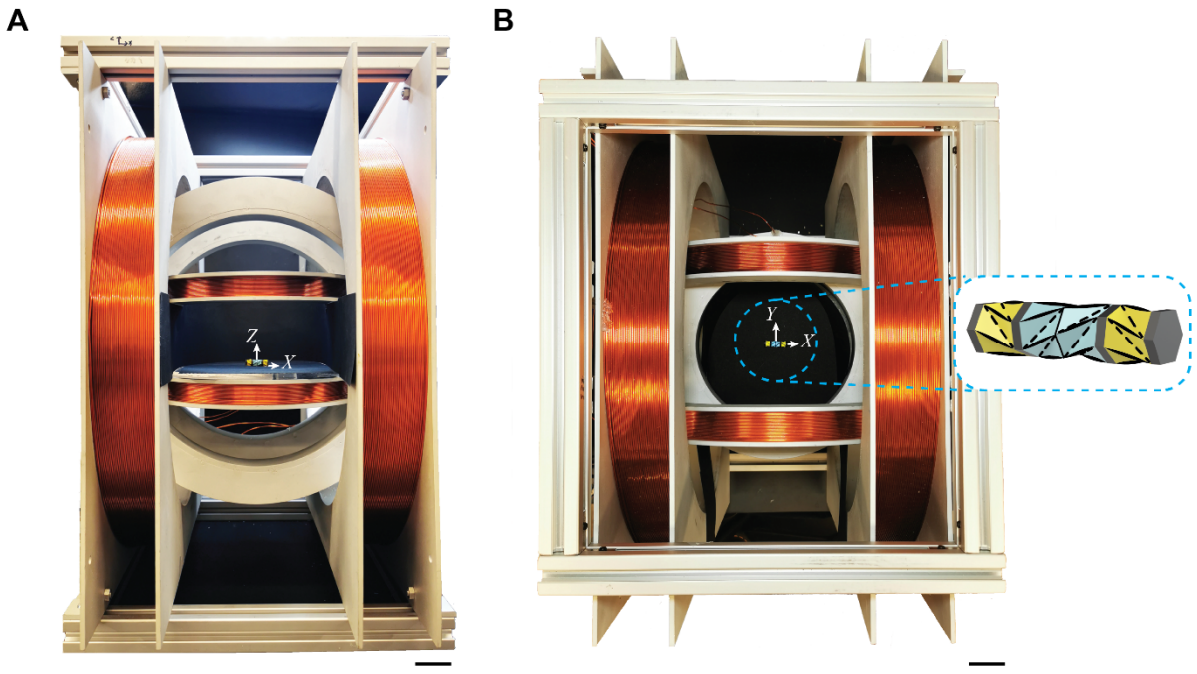

Fig. S7. 3D Helmholtz coils for magnetic actuation with the Kresling crawler inside the magnetic apparatus. (**A**) Front view. (**B**) Top view. Scale bars: 4 cm.

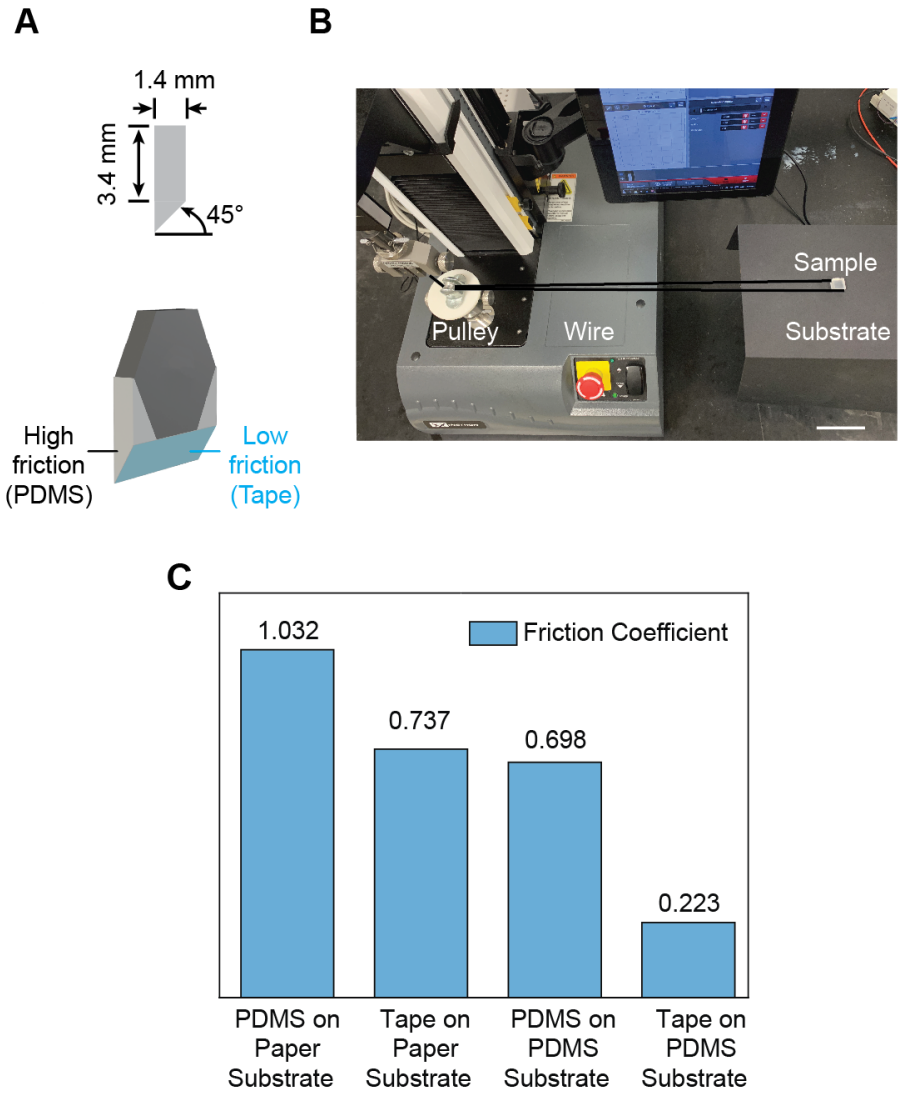

Fig. S8. Crawler feet design and friction coefficient measurement. (**A**) Dimensions of the feet and anisotropic friction design. (**B**) Experimental setup for friction coefficient measurement. Scale bar: 7 cm. (**C**) Measured friction coefficients between two materials (PDMS and tape) for feet design and two different substrates (paper and PDMS).

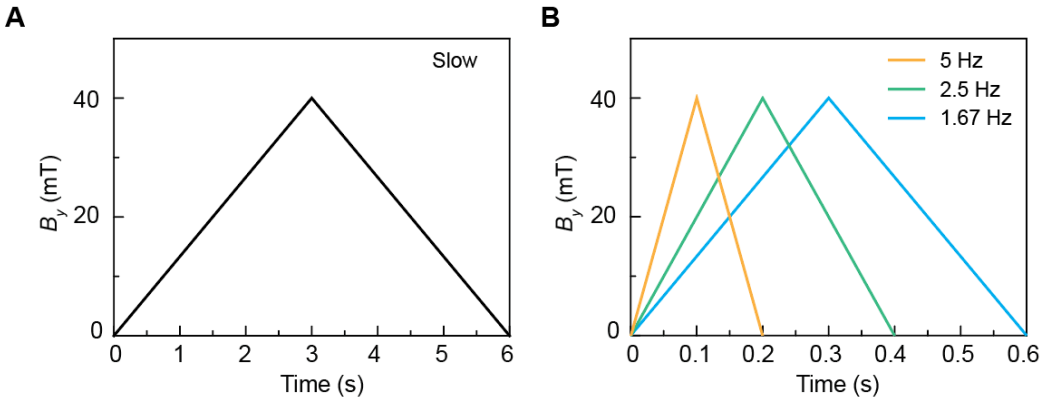

Fig. S9. Magnetic field profiles applied to the Kresling crawler. Magnetic field profiles for (**A**) relatively slow single stride to demonstrate the crawling mechanism and (**B**) relatively fast single stride with different frequencies for crawling motion characterization.

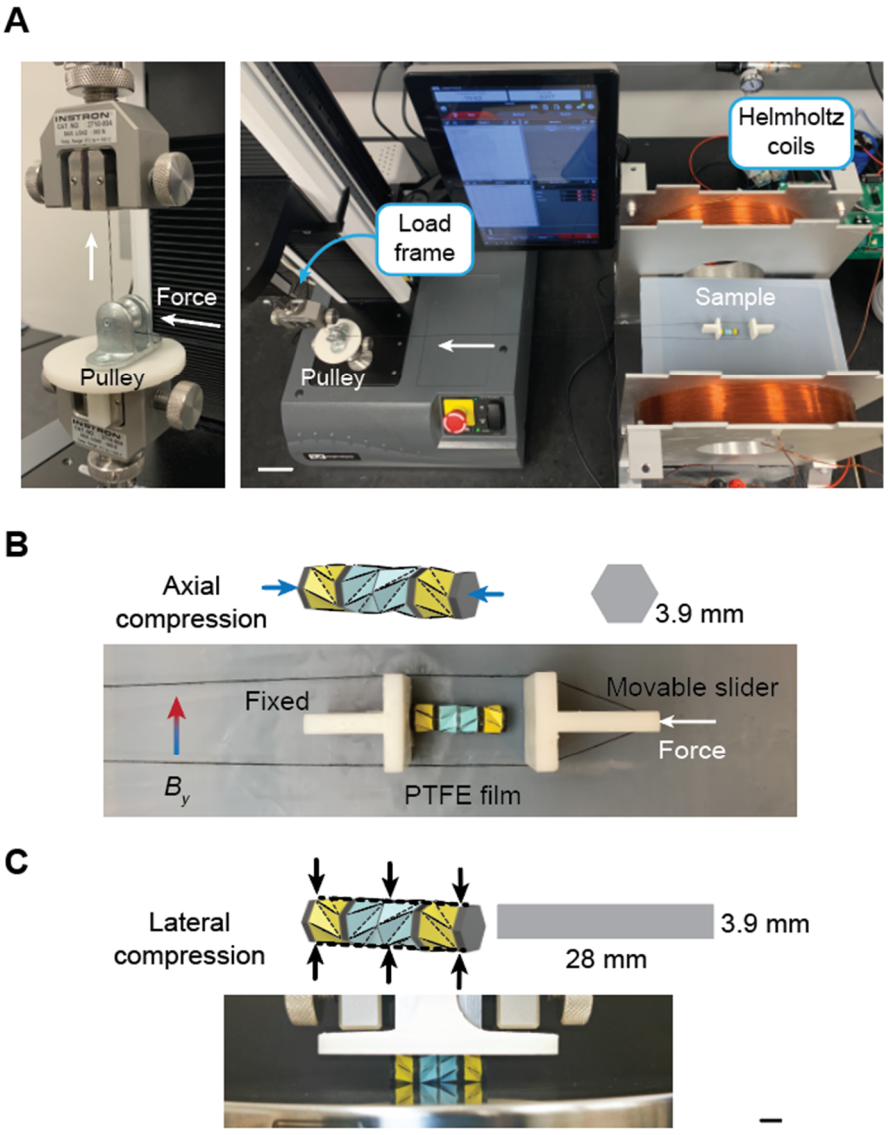

Fig. S10. Measurement of the anisotropic structure stiffness of the crawler body. (**A**) Experimental setup. To measure the axial stiffness of the crawler under magnetic fields, pulley and wire are used to transmit the force from the machine to a slider in the electromagnetic coils. The coils can provide a uniform magnetic field. Scale bar: 7 cm. (**B**) Schematics and experimental images of the compression tests along the axial direction. The positive magnetic field direction is identical to the net magnetization direction of the crawler. (**C**) Schematics and experimental images of the compression tests along the lateral direction. Scale bar: 5 mm.

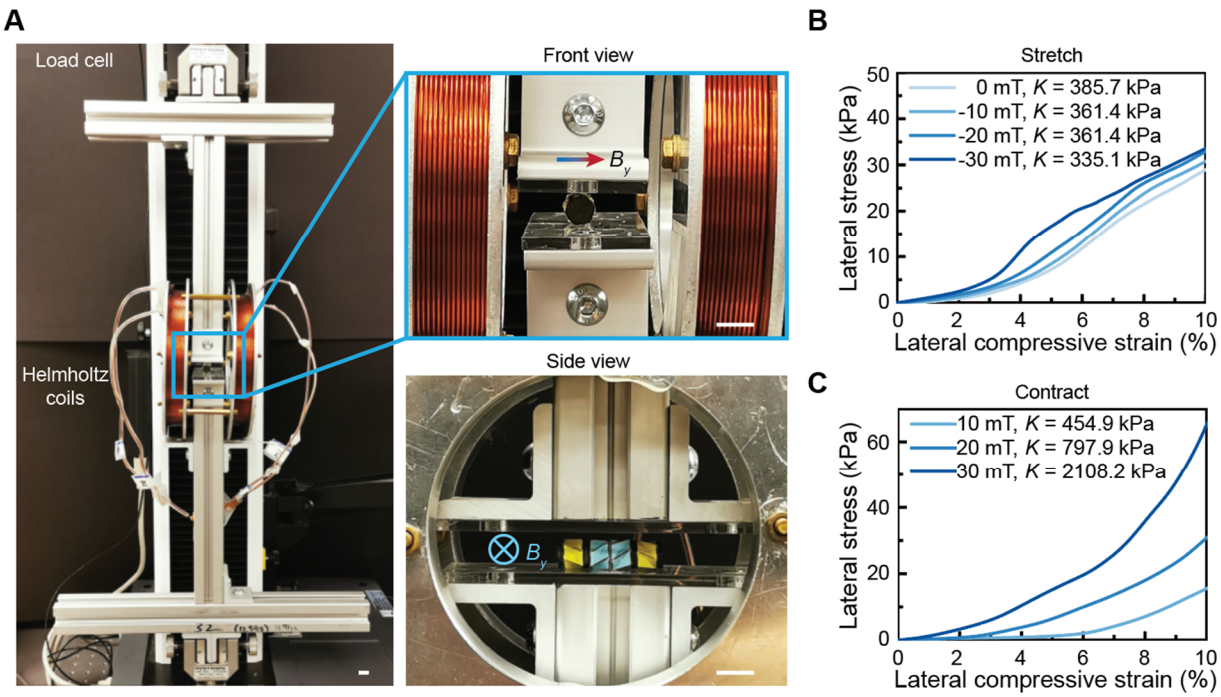

Fig. S11. Measurement of the lateral stiffness of the crawler body under different magnetic fields. (**A**) Experimental setup. The positive magnetic field direction is identical to the net magnetization direction of the crawler. Scale bars: 10 mm. Compressive stress-strain curves for the crawler along lateral direction under (**B**) negative magnetic fields and (**C**) positive magnetic fields. The crawler stretches under negative magnetic field (-10 mT, -20 mT, and -30 mT) and contracts under positive magnetic field (10 mT, 20 mT, and 30 mT). The stiffnesses are measured at the strain of 10%.

Table S1. Comparison between Kresling origami crawler and other crawling robots reviewed

Mechanism	Actuation	Robot design	Wireless control	Steering	Body length (BL, mm)	Weight (g)	Speed (BL/s)	Operation condition	Ref
Contractile structure	Magnetic	Four-unit origami assembly with two-level symmetry	Y	Y	28	0.95	0.47	5Hz, 40mT magnetic field	This work
	Motor	Two chiral origami towers	N	Y	150	136	0.025	0.4Hz, switch direction	[38]
		Six origami ball structure	N	N	603	220	0.02	0.1Hz, switch direction	[33]
	Pneumatic	Quadrupedal structure	N	N	150	-	0.05	1Hz, 7 psi pressure	[19]
		Elastomeric tube body with kirigami-enabled anisotropic frictional skin	Y	N	164	65	0.05	0.2Hz, Air volume change	[11]
	Thermal	Two four-bar mechanisms	N	Y	150	1.2	0.06	1Hz 0.35A current	[16]
		Tubular body with multiple origami segments	N	N	100	4.2	0.003	0.1Hz, 0.3A current	[29]
Stimuli-responsive materials	Magnetic	Four-cell structure with alternating magnetization and asymmetric joints	Y	N	60	2.4	0.56	3.3Hz, 30mT magnetic field	[12]
		Beam structure with multiple tapered feet	Y	Y	17	0.04	1.68	16Hz, 200mT magnetic field	[28]
	Thermal	Uniaxially oriented strip	N	N	35	0.08	0.03	0.06Hz, 0.577W power	[25]
		Strip with spatially modulated alignment pattern	Y	N	14.8	0.03	0.02	0.4Hz, 2.5W power	[17]
	Electrical	Prestretched dielectric elastomer membrane with a flexible frame	N	Y	85	-	1.04	25Hz, 6kV voltage	[3]
		Curved unimorph piezoelectric structure	N	N	10	0.024	20	850Hz, 200V voltage	[26]

Movie S1.
Contraction mechanism of the Kresling crawler.

Movie S2.
Crawling mechanism of the Kresling robot.

Movie S3.
Programmed motion of the Kresling crawler.

Movie S4.
Crawling in confined space and drug delivery.